Supplementary Materials for

Discretised microfluidics for noninvasive health monitoring using sweat sensing

Emma J.M. Moonen, Walther Verberne, Eduard Pelssers, Jason Heikenfeld, and Jaap M.J. den Toonder

Corresponding author: Jaap M.J. den Toonder, j.m.j.d.toonder@tue.nl

This PDF file includes:

Supplementary Text
Figs. S1 to S6
Movies S1 to S5

Other Supplementary Materials for this manuscript include the following:

Movies S1 to S5

Supplementary Text

Burst valve model

The burst valve model we have used to design the skin-device interface is schematically represented in Fig. 2A. We assume that a sweat gland behaves like a pump, generating a pressure P_g, and has a hydrodynamic resistance R_g. When sweat is generated by a sweat gland, the gap between the skin and the device will start filling. At that instant, the sweat flow rate equals the gland pressure divided by the gland's hydrodynamic resistance (P_g/R_g). The hydrodynamic resistance of the gland (R_g) is considerably larger than all other resistances in the system, due to its geometry (12). Therefore, as long as there is flow, the pressure drop over the gland is larger than over any other resistive component in the system. Consequently, the pressure at the bifurcation B, indicated in Fig. 2A, is very low during flow. After an initial filling time, the liquid pins at the two burst valves representing the inlet hole in the collection plate and the leakage gap between the skin and the device (ΔP_i and ΔP_L), because the available low pressure cannot overcome these valves. Consequently, the fluid flow will stop, and this has a profound effect on the local pressure at bifurcation B. The pressure drop over the sweat gland equals its hydrodynamic resistance (R_g) multiplied by the flow rate. As the flow rate becomes zero, the pressure difference drops to zero and consequently the pressure at B equals the full pressure of the gland (P_g). This means that the pressure generated by the sweat gland (P_g) is available to open one of the two burst valves, either ΔP_i or ΔP_L. If the pressure delivered by the gland (P_g) is sufficiently high, the burst valve which requires the lowest pressure will burst open, restoring a liquid flow and immediately the pressure at bifurcation B drops again to virtually zero. Consequently, the other burst valve with the higher burst pressure will not be opened. This mechanism only works if the lower burst pressure valve opens sufficiently fast; otherwise, the pressure remaining at the bifurcation may be significant enough to also trigger the opening of the higher burst pressure valve.

The initial condition that must be satisfied for successful entry of sweat into the inlet hole, as opposed to leaking between the skin and the device, is that the Laplace pressure for entry into the hole must be smaller than the Laplace pressure for leakage of sweat along the skin ($\Delta P_i < \Delta P_L$). Furthermore, the Laplace pressure for the sweat entering the inlet hole may not be larger than the pressure delivered by the sweat gland ($\Delta P_i < P_g$). The two conditions together are represented in Fig. 2B. A maximum pressure, delivered by the sweat glands, up to 70 kPa is reported in literature during chemical stimulation and under no flow condition (14, 15). A more recent publication of an experimental study found average values of secretory fluidic pressures generated at the surface of the skin by eccrine sweat glands in healthy young adults between 2.4 and 2.9 kPa, which is much lower (16). In our model, we use an average maximum pressure delivered by the sweat glands of 2.65 kPa.

The Laplace pressures in the system depend on dimensions of the device features, contact angles of the sweat with the different surfaces of the device, and the surface tension of the sweat. The Laplace pressures for entry of sweat into the inlet hole (ΔP_i), and respectively for leakage of sweat along the skin surface (ΔP_L) are given by:

$$\Delta P_i = \frac{-2\gamma\cos(\theta_i)}{r_i} \tag{S1}$$

$$\Delta P_L = \gamma\left(\frac{1}{r_i} - \frac{\cos(\theta_s) + \cos(\theta_i)}{h_L}\right) \tag{S2}$$

In these equations γ is the surface tension of sweat, θ_i is the contact angle of the collection plate, θ_s is the contact angle of the skin, r_i is the radius of the inlet holes in the collection plate, and h_L is the height of the gap between the skin and the collection plate. These parameters should be tailored to achieve successful sweat entry into the inlet hole, while suiting the dimensions of the sweat sensing device and the targeted body location.
Equation S2 describes the interface between the skin and the bottom of the collection plate as a capillary bridge with an equivalent height h_L, which represents the average distance between the skin surface and the collection plate. This representation is only valid when $h_L << r_i$ holds (27). Based on the average roughness of the skin at the intended body location and the method of application of the device to the skin, we have estimated this height h_L to be between 10 and 100 μm. Another important parameter that determines the Laplace pressure for leakage is the contact angle of sweat on the skin. The contact angle of sweat on the human skin depends on the skin location and the amount of sebum present on the skin and ranges between 40° and 75° (17). The material, and thereby wetting properties of the collection plate, can be different depending on the use case of the wearable sweat sensing device and the available fabrication techniques.

A solution space for the condition for successful entry of sweat in the inlet hole $\Delta P_i < \Delta P_L$ & P_g, is illustrated in Fig. 2B as created by solving Equations S1 and S2 for a contact angle of the non-hydrated skin (θ_s) between 40 and 75°, and a height between the skin and the collection plate (h_L) between 10 and 100 μm. The lines in Fig. 2B represent the boundaries for which $\Delta P_i = \Delta P_L$ for different radii of the inlet (r_i). Below this boundary, in the brown area, ΔP_i is larger than ΔP_L resulting in leakage of sweat over the skin. Above this boundary, in the blue area, ΔP_i is smaller than ΔP_L which results in successful entry of the sweat into the inlet hole. For all the parameters represented in this solution space, the required pressure for sweat entering the inlet holes (ΔP_i) remained below the average maximum pressure delivered by the sweat glands (P_g) of 2.65 kPa.

To keep the filling volume of the sweat sensing device low, both the inlet hole radius ri and the distance between the skin and the device (hL) must be as small as possible. However, Fig. 2B shows that for a small height hL combined with a realistic contact angle of the skin around 50-60°, the Laplace pressure for leakage (ΔPL) is lower than the Laplace pressure for entry (ΔPi) even for larger ri, resulting in leakage. Therefore, simply placing the collection plate directly on top of the skin, possibly resulting in hL as small as 10 μm, will not result in successful entry of sweat into the device. To solve this problem, we have implemented two solutions: attaching a hydrophobic (θ = 102°) double- sided medical tape with thickness 80 μm to the collection plate, which conforms to the skin and thus reduces gap height (hL) which is estimated at 10 μm, and applying petroleum jelly on the skin before attaching the device, which increases the contact angle of sweat on the skin to θs=102°, and thereby increases the Laplace pressure for leakage (ΔPL) significantly. Indeed, Fig. 2B shows that for such a high θs, inlet hole entry will be successful even for small hL and ri. Hence, by using this solution, the dead volume is kept low by maintaining a small gap between the skin and the device (hL), but the Laplace pressure for leakage (ΔPL) is still larger than the Laplace pressure for entry (ΔPi) due to an increase of the contact angle of the skin (θs). As these solutions do not influence the pressure required for entry into the collection hole (ΔPi), it remains lower than the pressure the gland can deliver (Pg). The introduction of the double-sided medical tape also creates the possibility to increase the sampling area while keeping the filling volume low, by choosing a larger radius of the hole in the tape than the radius of the hole in the collection plate. If the radius in the double-sided medical tape is larger than the radius of the hole in the collection plate r_t, Equation S2 is adapted to:

$$\Delta P_L = \gamma\left(\frac{1}{r_t} - \frac{\cos(\theta_s) + \cos(\theta_i)}{h_L}\right) \quad \text{(S3)}$$

In this equation r_t is the radius of the hole in the tape. After entry into the inlet hole in the collection plate, the sweat needs to bulge out on top of the hole and touch the ceiling of the EWOD chamber for entry into the device. It is essential that the Laplace pressure for bulging of sweat into the EWOD chamber is smaller than the Laplace pressure for leakage of sweat along the skin ($\Delta P_c < \Delta P_L$). Furthermore, the Laplace pressure for the sweat entering the EWOD chamber may not be larger than the maximum pressure delivered by the sweat gland ($\Delta P_c < P_g$).
The Laplace pressure for bulging of sweat out of the inlet hole into the EWOD chamber (ΔP_c) is equal to:

$$\Delta P_c = \frac{-2\gamma\cos(\theta_c)}{r_i} \quad \text{(S4)}$$

The bulging angle θ_c of the liquid once it reaches the top of the EWOD chamber can be calculated from the geometry, shown in Fig. 2A, using the following equation:

$$\theta_c = -2\tan^{-1}\left(\frac{h_c + r_i}{h_c - r_i}\right) \quad \text{(S5)}$$

In this equation h_c is the height of the EWOD chamber. The maximum bulging angle is equal to 180° and therefore this equation is only valid when $h_c < r_i$.

A solution space for the condition for successful entry both into the inlet hole and in the EWOD chamber ΔP_i & $\Delta P_c < \Delta P_L$ & P_g, is illustrated in Fig. 2C. Equations S1 and S3-S5 are solved for a radius of the inlet (r_i) between 40 and 80 µm, and a height between the skin surface and collection plate (h_L) between 10 and 100 µm. The contact angle of the skin (θ_s) is fixed at 102°, which is the contact angle of sweat on a skin surface with petroleum jelly. The pressure delivered by the sweat gland P_g is again set at 2.65 kPa. The radius of the hole in the tape is taken to be equal to the radius of the hole in the collection plate ($r_t = r_i$).
The lines in Fig. 2C represent the boundaries for which ΔP_i & $\Delta P_c < \Delta P_L$ & P_g does not hold anymore for different heights of the EWOD chamber (h_c) between 10 and 40 µm. In between these lines, in the blue area, ΔP_i and ΔP_c are both smaller than both ΔP_L and P_g, resulting in successful entry of sweat into the inlet hole and subsequently into the EWOD chamber. Outside the lines, in the brown area, ΔP_i & $\Delta P_c < \Delta P_L$ & P_g is not valid, which results in leakage of sweat over the skin, and/or blocking of the sweat glands because the Laplace pressure for entry into the hole (ΔP_i) or into the EWOD chamber (ΔP_c) cannot be delivered by the sweat glands.
By lowering the EWOD chamber height (h_c), the Laplace pressure for bulging into the chamber (ΔP_c) increases which can lead to a Laplace pressure above the maximum pressure delivered by the sweat gland (P_g) when the radius of the inlet (r_i) is too small. When the height of the EWOD chamber (h_c) is larger than 20 µm, the Laplace pressure for bulging into the chamber (ΔP_c) is smaller than the maximum pressure delivered by the gland (P_g) for all radii of the inlet hole (r_i) between 40 and 80 µm. Increasing the radius of the inlet holes (r_i) leads to a decrease in the Laplace pressure for leakage (ΔP_L) which can lead to it being lower than the Laplace pressure for entry into the holes (ΔP_i) or bulging into the EWOD chamber (ΔP_c) when the height between the skin and the device (h_L) is too large.

Use of petroleum jelly

We designed a test device to experimentally verify the findings of the analytical model presented in the earlier section. This test device, schematically represented in Fig. 1a, is designed to detect the entry of sweat through the collection plate. The device consists of a collection plate covered with a metal coating and a hydrophobic coating (AF1600), and a glass slide with column electrodes covered with a dielectric material (Parylene C) and a hydrophobic coating (AF1600). These are attached to each other with a patterned dry film resist layer and double-sided tape to form a chamber. The holes in the collection plate are aligned with the column electrodes, and when sweat protrudes from an inlet hole and touches the top of the chamber, a change in the capacitance between the column electrodes and the collection plate electrode is detected. Depending on the desired application of the sweat sensing device, this test device can be adapted to test different dimensions and wetting properties.

The results presented in this section are obtained with a device of which the dimensions are depicted in fig. S1A. The current test device consists of a glass collection plate with a thickness of 100 µm with 162 holes with a radius of 45 µm. The radius of the holes in the hydrophobic tape (r_t) is equal to 150 µm, which leads to a radius of the sampling surface (r_s) of 175 µm by adding the radius of the sweat gland (r_g). Both glass slides are coated with hydrophobic coating with a contact angle of 110°. The chamber has a height of 25 µm and contains 9 column electrodes. Using Equations S1, S4 and S5, these dimensions result in a Laplace pressure for entry of sweat into the hole (ΔP_i) of 1.05 kPa and a pressure for bulging of sweat into the chamber (ΔP_c) of 2.61 kPa. Assuming a height (h_L) between the skin and the collection plate of 10 µm, the Laplace pressure of leakage of sweat between the skin and the device (ΔP_L) is expected to be -1.14 kPa according to Equation 2 when the skin contains sebum and 4.27 kPa when petroleum jelly is applied. Consequently, successful entry of sweat is expected only when petroleum jelly is applied, because then ΔP_i & $\Delta P_c < \Delta P_L$ & P_g is true.

The test device is placed on the fingertip of a person in resting state. The entry of sweat can be detected by an increase of the capacitance of the electrodes over time. Fig. S1B shows the measured capacitance of the different column electrodes as a function of time when no petroleum jelly is applied on the surface of the skin. The measured capacitance does not increase significantly, which confirms that no sweat enters the test device as predicted by our model. After 15 minutes, the device was inspected under the microscope which confirmed that no sweat had entered the device. Fig. S1C shows the measured capacitance as a function of time for a device which is placed on the fingertip after application of petroleum jelly on the skin. The different lines represent the measurements from the different column electrodes. The electric connection to one of the electrodes failed and therefore only eight of nine are displayed. The capacitance of the electrodes increases with time which indicates the entry of sweat, which was confirmed by inspection under the microscope. This result is again in agreement with the model predictions. Depending on the number of active sweat glands, a certain number of sweat glands is sampled. The detected capacitance is not the same on each electrode as it is dependent on the surface area covered with sweat, and thus on the number of sweat glands that are sampled by the inlet holes below each column electrode.

Methods

Electrode layer fabrication

Microscope glass slides (25x75mm) were cleaned in an ultrasonic cleaner for 15 minutes in subsequently 2% soap solution (Micro-90) and 90-10% isopropanol-acetone solution. The slides were baked for 1 hour at 120 °C to eliminate any moisture. After cooling down, the surface was activated using a 15-minute UV ozone treatment (Novascan, PSD series). Photoresist AZ nLof 2035

(Microchemicals) was spincoated, baked for 3.5 minutes at 100 °C, exposed using a film photomask, baked for 1 minute at 120 °C, and developed in AZ 726 MIF developer (Microchemicals) for 45 seconds. Au electrodes were formed by sputtercoating (Quorum Q300TD) of Cr (5 nm) and Au (50 nm) and subsequent lift off in Technistrip NI555 (Microchemicals) at 70 °C. Ordyl SY320 dryfilm photoresist (Microchemicals) was laminated (GBC laminator) at 50 °C, aligned and exposed (MJB4, Suss Microtec) and developed in K45 developer (Microchemicals). A 1.1 µm thick layer of Parylene C was deposited by chemical vapour deposition (Labcoter, Speciality Coating Systems). During the deposition, the contact pads were shielded with Parafilm. Finally, a layer of AF1600 1 wt% in FC70 (Merck Life Science) was spincoated at 2000 rpm and baked at 70 °C for 1 hour.

Collection plate fabrication

Holes were defined in 100 µm thick glass using laser drilling (Micronit). The conductive coating was defined by sputtercoating (Quorum Q300TD) of Cr (2 nm) and Au (9 nm). A layer of AF1600 1 wt% in FC70 (Merck Life Science) was spincoated at 2000 rpm and baked at 70 °C for 1 hour.

Alignment and assembly

A 25 µm thick spacer tape (ARcare 92734, Adhesives Research) was cut using a CO2 lasercutter (VLS 3.50, Universal Laser Systems). The tape was manually aligned on the electrode layer, and the collection plate and electrode layer were aligned and bonded using a mask aligner (MJB4, SUSS MicroTec). Conductive ink (Electric paint, bare conductive).

Sweat gland distribution

It is assumed that sweat glands are randomly and independently distributed. In this case, a Poisson distribution can be used to calculate the probability of a certain number of sweat glands being present in a collection area with size A_c. The number of sweat glands present on the fingertips reported in the literature varies between 100-1000/cm^2 (13, 28). It is assumed that in sedentary state about 10% of these glands are active. Therefore, we have used our model to calculate the probabilities based on an active sweat gland density of 10, 50 and 100 glands/cm^2. The probability P_n that n glands are present in a sample area of size A_s is given by:

$$P_n = \frac{\lambda^n}{n!} e^{-\lambda} \quad \text{(S6)}$$

In this equation, λ is the average number of glands in the area As, which can be calculated by multiplying A_s with the average gland density G_d: $\lambda = A_s G_d$. A sweat gland centre which is positioned adjacent to the hole in the tape will still be able to supply the hole with sweat. This means that the total sampling radius per hole is equal to the radius of the hole in the medical tape, plus 25 μm, which is taken as the radius of the sweat gland (12). In our final design shown in Fig. 2D-G, the total sampling radius per collection chamber is therefore 175 μm, and we have a total number of 50 collection chambers per quadrant and 4 quadrants; therefore, the sampling area of one quadrant is 0.048 cm^2, and the total sampling area is A_s=0.192 cm^2.

Fig. S2A shows the probability of sampling 0, 1 or more than 1 sweat glands per collection chamber with sampling radius 175 μm, for different active gland densities. Most collection cambers are empty, some will contain one sweat gland and the probability that more than one sweat gland is sampled in a single collection chamber is very low for all three cases, namely less than 0.5%. fig. S2B shows the probability of the total number of glands being sampled, for the final design of the collection plate shown in Fig. 2D-G, i.e., with 200 collection chambers. The average number of glands sampled by the wearable device is respectively ±2, ±10, and ±19 for 10, 50, and 100 active glands/cm2. For the fingertip of individuals at rest, 50 active glands/cm^2 is a reasonable value which means that ±10 glands will be sampled by our device.

Finally, it is important to calculate the probability of no glands occurring in neither of the collection areas (P_0^N); for all cases this probability is maximally 0.0045% which is acceptable in clinical applications.

Sub-nanolitre droplet EWOD actuation

We experimentally tested the pinching and transport of sub-nanolitre droplets, using the two-step design presented in fig. S3A DI water is used as actuation liquid in the experiments presented in this subsection, as this is a commonly used liquid in EWOD experiments and serves as a means to prove the actuation of sub-nanolitre droplets. A larger droplet is pinched from the first reservoir, and it is transported to the second set of reservoir electrodes. fig. S3B shows a time-lapse, with a time step of 0.5 seconds, of a droplet being pinched and transported from the reservoirs in the second step towards the waste electrode. The electrodes are charged with 80 V_{AC} at a frequency of 1 kHz. The sequence in which the electrodes are turned on and off is essential for successful droplet pinching. When an electrode is turned off it is connected to ground, which is important for discharging the electrode. In fig. S3B the actuation, on (green) or off (black), of the electrodes is indicated below each image. First, the big reservoir electrode (R1) is turned on, which aligns the droplet to the middle of the reservoir and thus to the EWOD chamber. It is essential that the droplet is not larger than the large reservoir electrode (R1), because the reservoir electrode aids the pinching of a droplet in the subsequent steps by providing a pulling force. If the droplet is larger than this reservoir electrode (R1), the pulling force will not be delivered. Next, the large reservoir (R1) is turned off and the small reservoir (R2) and subsequent three path electrodes (P1-3) are turned on, which pulls the liquid through the opening in the dry film structures over the path electrodes. When the smaller reservoir electrode (R2) is turned off, the liquid fully extends over the first three path electrodes (P1-3). Next, the first 2 path electrode (P1-2) are turned off while simultaneously the large reservoir electrode (R1) is turned on to achieve successful pinching of a droplet. The resulting pull from the big reservoir electrode (R1) retracts the liquid, but the portion of the big droplet on the path electrode which is still on (P3) remains, thereby resulting in a smaller droplet being pinched from the large droplet which remains on the reservoir. By subsequently actuating the next path electrodes, the droplet gets transported towards the waste electrode. The volume of this droplet was calculated to be 50 pL, based on measuring the surface area of this droplet on the waste electrode.

Signal analysis

Using the amplification circuit depicted in Fig. 4A, the output capacitance of the sensor can be calculated using the following equation:

$$\left|V_{out}\right| = \left|V_{in}\right| \frac{C_{sensor}}{C_f} \tag{S7}$$

The choice of C_f and R_f determine the lower cut off frequency of the amplifier, effectively serving as a high-pass filter. The measurement frequency should be higher than the lower cut off frequency f_{hpf}, which can be calculated using the following equation:

$$f_{hpf} = \frac{1}{2\pi R_f C_f} \tag{S8}$$

The sensing circuit was modelled using LTspice. Fig. S5a shows the frequency response of the circuit with C_f = 300 pF, R_f = 470 kΩ and V_{in} = 5 V_{AC}. Based on this frequency response, we use a measurement frequency of 5 kHz, because this frequency is higher than the cutoff frequency around 3 kHz.

A preliminary analysis was performed to determine whether the variation in the droplet size, corresponds to the experimentally measured capacitance output. Using ImageJ 12 images (fig. S5B) of measurements are analysed to determine the percentage of the sensor electrode that is covered with water. An estimation is made of the shape of the droplet on the electrode, because these images are taken from the top side and

the droplet is located below the electrode. Fig. S5C shows the sensor coverage as a function of the measured capacitance. A linear correlation can be seen, which means that the measured capacitance indicates the percentage of the sensor electrode covered with liquid. By using this linearity an estimation of the droplet size can be made from the measured capacitance. Analysing the sensor signal to determine the volume of individual droplets makes the calculation of flow rate from droplet count more reliable.

Electronic system and interface design

A dedicated setup is used for actuation of the wearable sweat sensing device and acquisition of the sensor signals. The electronic system, schematically depicted in fig. S4A, contains three main parts: the control printed circuit board (PCB), the actuation and signal acquisition hardware, and two computers. The control PCB (fig. S4B) is the central component of the setup. It contains relays, the measurement circuit which is explained in the earlier section including the power supply for the operational amplifier (opAmp), a current limiter, and a microcontroller to control the switching of the relays. Furthermore, the control PCB has connectors for connecting the actuation and signal acquisition hardware. This hardware consists of a waveform generator for providing the AC actuation (V_a) and sensing (V_s) signals, an amplifier to amplify the actuation signal, a data acquisition unit (DAQ) for acquiring the sweat sensor signals and a multimeter for monitoring the leakage current (I_L), which is the current that flows from the EWOD electrodes to the ground collection plate electrode. Finally, the control PCB also has two connectors for connecting the wearable sweat sensing device via a dedicated cable.

The final EWOD layer design of the wearable device, shown in Fig. 3C, consists of 37 groups of EWOD electrodes and 2 connection pads for the collection plate electrode. Using anisotropic conductive film (ACF) bonding a PCB with an integrated flexible part is aligned and attached to the electrode pads on the glass of the EWOD layer. In the current setup, two separate PCs are used, one for controlling the microcontroller and acquiring the multimeter signals and one for acquiring the sweat sensor signals via the DAQ. If a PC with enough random-access memory (RAM) is used, both processes can be operated on the same PC. A photograph of the full setup, excluding the control PC, can be seen in fig. S4C.

The timing of the switching of the relays is essential for the successful operation of the device; Fig. 4B presents a schematic overview of the timing of the relays. These relays are all identical components, but serve three different purposes in controlling the wearable device: 37 actuation relays for switching the groups of electrodes, one source selection relay for switching the input signal between the actuation signal (80 V, 0.4 kHz) and the measurement signal (5 V, 5 kHz), and one collection plate relay for switching the collection plate between ground, during EWOD actuation, and the measurement circuit, during sweat rate sensor measurements. The sensor relays are the same relays as the electrode relays. The electrodes are charged in groups of two, as COMSOL simulations confirmed that this actuation sequence resulted in optimal conditions for pinching droplets. Each set of electrodes is charged for 460 ms, then the electrode relays are switched off, the actuation control relay switches to the measurement signal and the collection plate relay switches to the measurement circuit. During the next 40 ms each of the four sweat rate sensors is switched on sequentially for 10 ms and the data is logged via the DAQ to the acquisition PC.

The DAQ is triggered using a hardware trigger (V_t) connected to the collection plate relay; when this relay is switched the DAQ records 40 ms of data. Using software on the acquisition PC this 40 ms is then separated into four times 10 ms and analysed to acquire the capacitance. This sequence is repeated five times to complete one wave. In normal operation the leakage current (IL) that flows through the device is below 200 μA, due to the high resistance of the dielectric layers. However, as a voltage of 80 V is used on a device placed on the skin, a current limiter is implemented in the hardware of the control PCB. This current limiter will limit the current when the resistance of the device decreases, for instance in the case of a shortcut of the 80 V to the skin. Fig. S4D shows a schematic diagram of the current limiter based on two depletion-mode MOSFETs and a resistor. The resistance determines the limit of the current and is currently set to limit currents above 0.75 mA. Fig. S4E shows the results from an LTspice model demonstrating the current limiting. In normal operation of the wearable sweat sensing device the resistance to the skin is high, in the order of MΩ, represented by the blue lines. The green lines represent the case when there is a shortcut to the skin and the resistance decreases to 10 kΩ. The top graph displays

the voltage (dashed line) and the current (solid line) in the situation without the current limiter. When the resistance to the skin decreases (green lines), the current increases to currents as high as 10 mA. The bottom graph displays the situation when the current limiter is implemented. In this case, when the resistance to the skin decreases (green lines), the current (solid line) is capped at a safe level. When the current is being limited by the current limiter, an LED is activated to notify the operator.

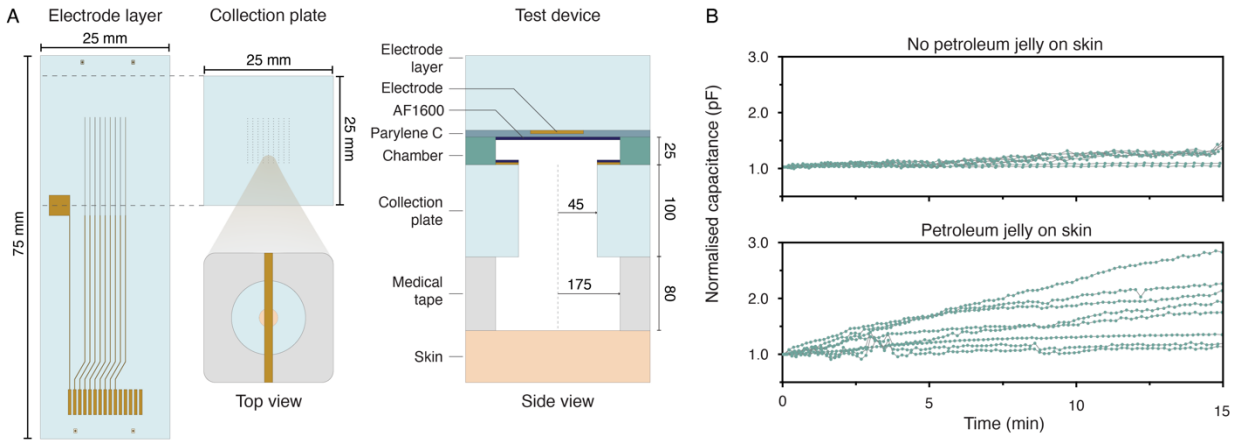

Fig. S1. Test device for the verification of the entry of sweat into the device. (A), Electrodes are patterned on a glass slide and covered with Parylene C. A collection plate with holes and a conductive and hydrophobic coating is aligned and attached to this glass slide using an intermediate layer of dry film resist and double-sided tape, forming a chamber. When sweat enters through the holes in the collection plate and touches the electrodes on top of the chamber, a change in capacitance is measured between the top column electrode and the bottom collection plate electrode. The device is attached to the skin using medical tape. Dimensions are indicated in µm unless noted otherwise. **(B)**, Measured electrode capacitance as a function of time for sweat collection measurements. The test devices are placed on the fingertip of an individual in rest with and without petroleum jelly on the skin. The experimental results correspond to the predictions by the model presented in the supplementary text. Note that only a limited number of sweat glands are covered by the test device and therefore it is plausible that the capacitance detection of the different electrodes is not the same, as the quantity of sweat is not the same.

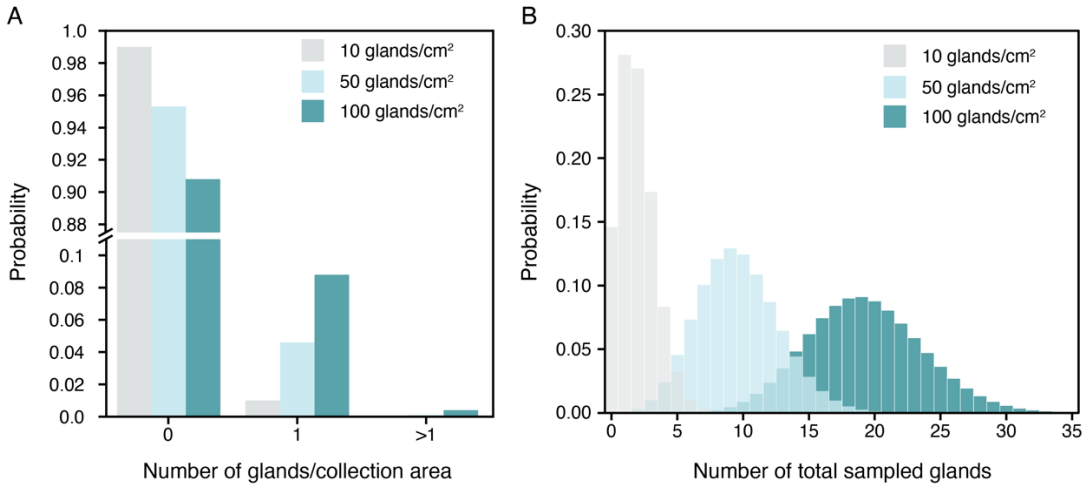

Fig. S2. Poisson distribution of the number of sampled glands. (A), Chance of sampling 0, 1 or more than 1 gland per collection chamber for 10, 50 or 100 active glands/cm^2; the collection area per chamber has a sampling radius of 175 µm. Most collection chambers will be empty, some will contain one sweat gland and the probability that more than one sweat gland is sampled in a single collection chamber is in all three cases less than 0.5%. The y-axis contains a break from 0.1 to 0.88. **(B)**, Probability distribution functions of the number of sampled glands in 200 collection chambers each with a sampling radius of 175 µm, corresponding to a collection area of 0.0962 mm^2. The average number of glands sampled by the wearable device is respectively ±2, ±10, and ±19 for 10, 50, and 100 active glands/cm^2.

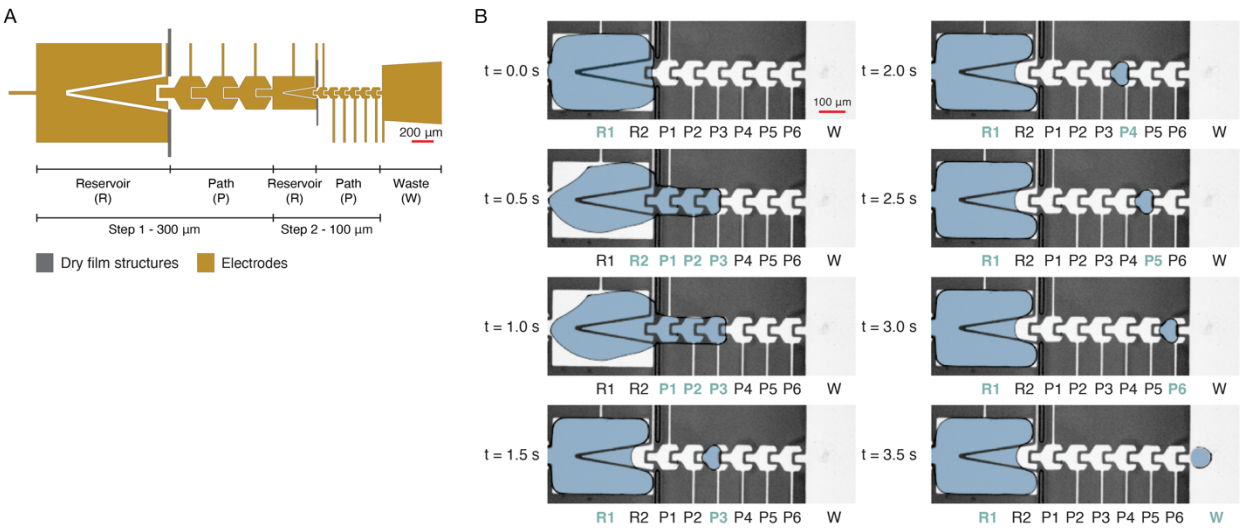

Fig. S3. Pinching and transport of sub-nanolitre droplets. (A), Two-step electrowetting test device design consisting of two sets of two reservoir electrodes (R), three and six path electrodes (P) and one waste electrode (W). Two dry film structures are placed next to the reservoir electrodes to aid the pinching of droplets. The width of the path electrodes in steps 1 and 2 are equal to 300 µm and 100 µm, which results in a 9-fold reduction of droplet volume from step 1 to step 2 from 0.71 nL to 0.079 nL. **(B)**, Time-lapse of a sub-nanolitre droplet of DI water being pinched from the reservoir electrodes (R1 and R2) and transported on 100 µm path electrodes (P1-P6) towards the waste electrode (W). The symbols below the images illustrate which electrodes are turned on (green) or off (black). The time step is equal to 0.5 seconds. The liquid is coloured in post-processing to increase the visibility.

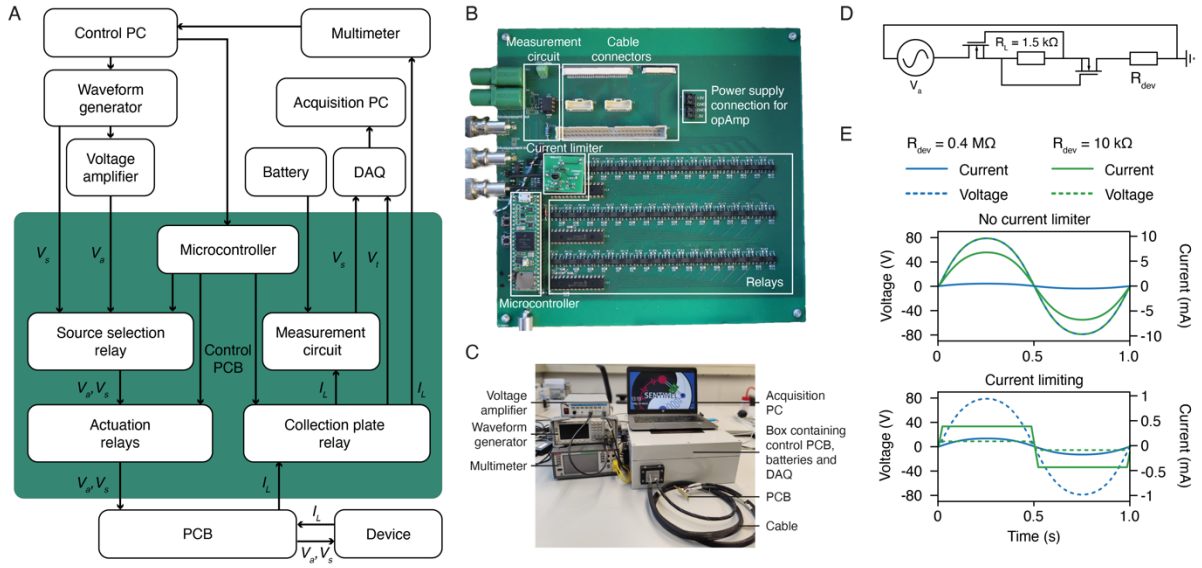

Fig. S4. Electronic system and interface design. (A), System-level block diagram of the electronic design. The elements in the green area are embedded in the control PCB. V_s and V_a represent the sensing and actuation signal and I_L represents the current that is recorded from the collection plate electrode. **(B)**, Photograph of the control PCB containing the measurement circuit, the microcontroller, the current limiter, the relays, the connectors for the cable towards the sweat sensing device and connectors to the waveform generator, multimeter, amplifier, DAQ and PC. **(C)**, Photograph of the full set-up. The box contains the control PCB, the batteries and the DAQ. The cable with the PCB which connects to the device is placed in front of the box. The control PC is not included in the photograph. **(D)**, Schematic diagram of the current limiter based on two depletion-mode MOSFETs and a resistor. The resistance determines the limit of the current and is currently set to limit currents above 0.75 mA. A current limiter is implemented in the electronic system to minimise the risk of electric shock of the user of the wearable sweat sensing device. **(E)**, Results from an LTspice model demonstrating the current limiting. In normal operation of the wearable sweat sensing device the resistance to the skin is high, in the order of MΩ, represented by the blue lines. The green lines represent the case when there is a shortcut to the skin. The top graph displays the voltage (dashed line) and the current (solid line) in the situation without the current limiter. When the resistance to the skin decreases, the current increases to values as high as 10 mA. The bottom graph displays the situation when the current limiter is implemented. In this case, when the resistance to the skin decreases, the current is capped at a safe level.

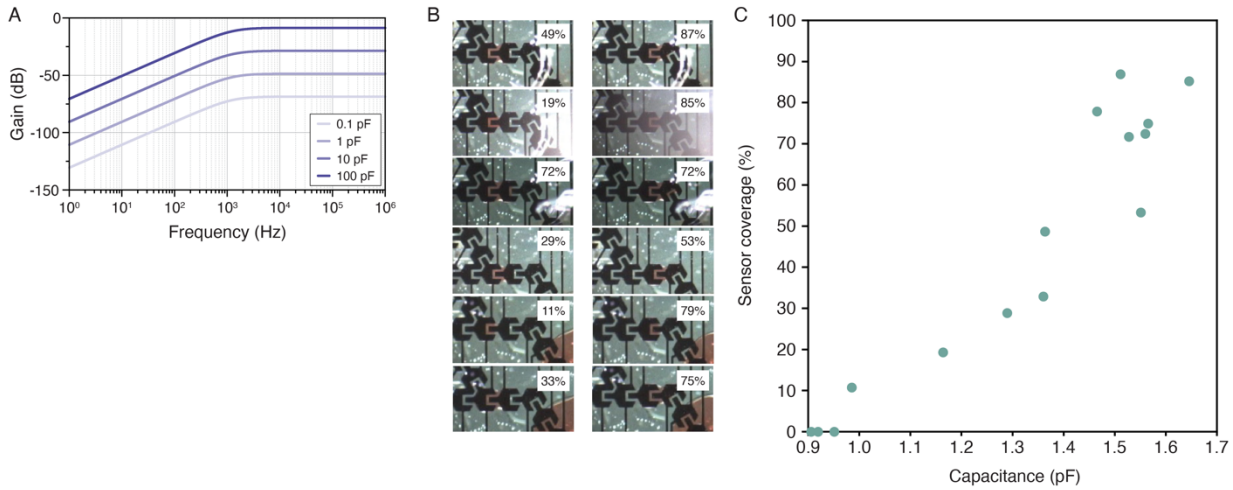

Fig. S5. Sweat rate sensor analysis. (A), Frequency response of V_{out} of the sensor circuit modelled in LTspice. A measurement frequency of 5 kHz is used, which is higher than the cutoff frequency of the high-pass filter. A change in capacitance (0.1-100 pF) can clearly be noted by an increase in the magnitude of V_{out}. **(B, C)**, Relationship between measured capacitance and droplet volume. **(B)**, Analysed images of six droplets passing over the sensor electrode. Using ImageJ, the percentage area covered by the droplet is estimated. **(C)**, Sensor coverage versus measured capacitance. Each of the data points corresponds to one of the images. A linear correlation can be seen, which indicates that an estimation of the droplet size can be made from the measured capacitance.

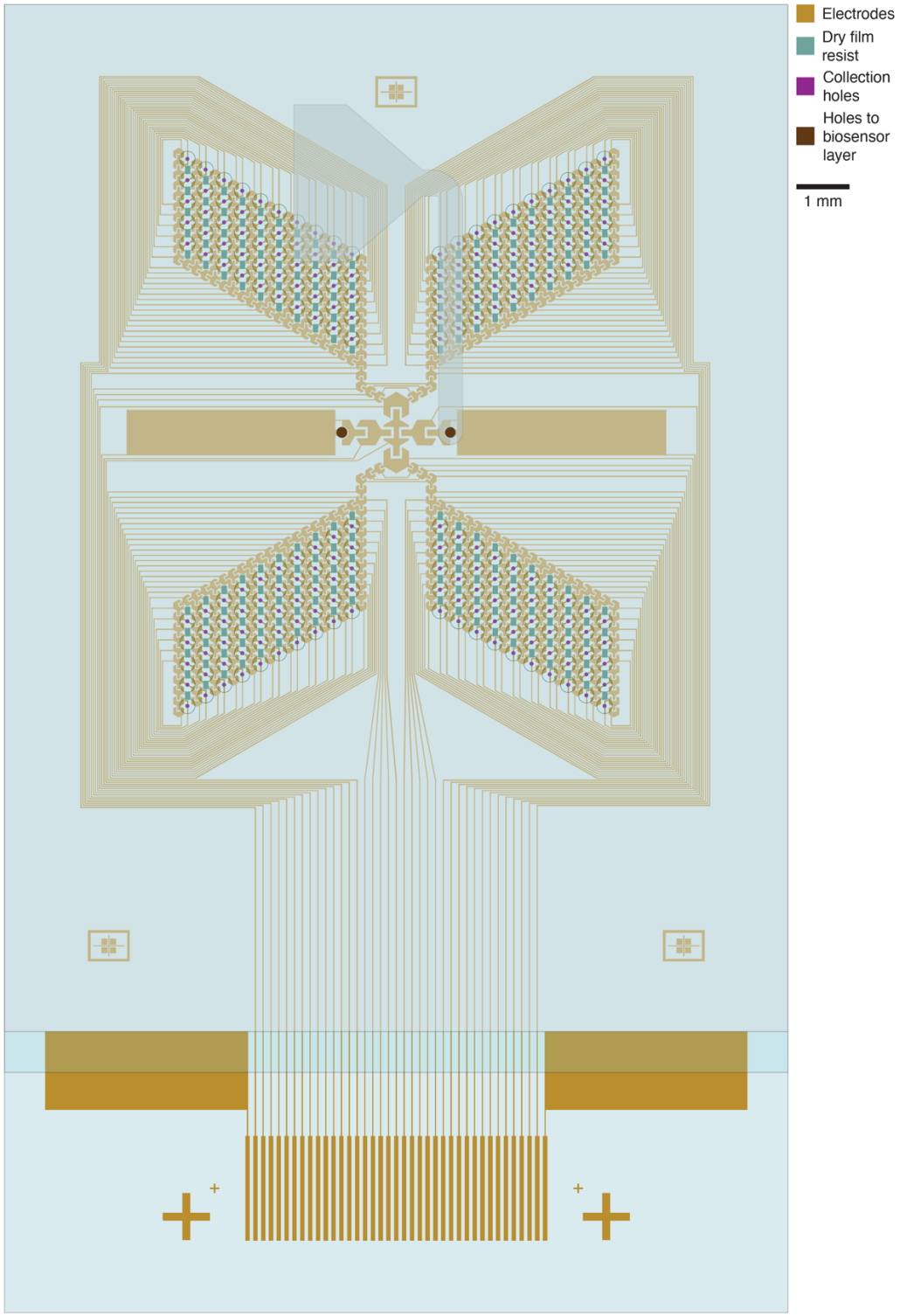

Fig. S6. Design of the integrated device including all layers.

Movie S1. Movie displaying the pinching of a droplet of coloured DI water from an active inlet hole, with a step size of 0.5 seconds. The liquid enters from the active inlet hole, and once it is grown to have enough overlap with the EWOD electrodes it gets pinched. The EWOD transport then moves the droplet to the right, where the sweat rate sensor is located (out of view).

Movie S2. Movie displaying the transport of a droplet of coloured DI water with a step size of 0.1 seconds. The EWOD transport velocity can be as high as 100 ms per step, reducing the time from collection to sensing and minimising the effect of evaporation.

Movie S3. Movie displaying the filling and emptying of the biosensor chamber from the outlet hole. The biosensor chamber can be emptied completely by the waste absorber. This leads to discretised biosensor measurements which are not averaged over time.

Movie S4. Movie displaying the passing of droplets over the sensor in a device placed on human skin. A sequence of five sweat droplets gets transported towards the middle of the device (top right), where the sweat rate sensor is located.

Movie S5. Movie displaying the operation of a device on human skin at a higher sweat rate. The quality of the movie is limited due to recording on a person. This movie shows the device can collect, pinch and transport droplets of real sweat on-body.